Human Molecular Genetics, 2014, Vol. 23, No. 18 **4786–4800**
doi:10.1093/hmg/ddu194
Advance Access published on April 29, 2014

Rapid depletion of muscle progenitor cells in dystrophic *mdx/utrophin*$^{-/-}$ mice

Aiping Lu, Minakshi Poddar, Ying Tang, Jonathan D. Proto, Jihee Sohn, Xiaodong Mu, Nicholas Oyster, Bing Wang and Johnny Huard*

Department of Orthopaedic Surgery, University of Pittsburgh, Pittsburgh, PA 15219, USA

Received December 10, 2013; Revised March 27, 2014; Accepted April 24, 2014

Duchenne muscular dystrophy (DMD) patients lack dystrophin from birth; however, muscle weakness becomes apparent only at 3–5 years of age, which happens to coincide with the depletion of the muscle progenitor cell (MPC) pools. Indeed, MPCs isolated from older DMD patients demonstrate impairments in myogenic potential. To determine whether the progression of muscular dystrophy is a consequence of the decline in functional MPCs, we investigated two animal models of DMD: (i) dystrophin-deficient *mdx* mice, the most commonly utilized model of DMD, which has a relatively mild dystrophic phenotype and (ii) dystrophin/utrophin double knock-out (dKO) mice, which display a similar histopathologic phenotype to DMD patients. In contrast to age-matched *mdx* mice, we observed that both the number and regeneration potential of dKO MPCs rapidly declines during disease progression. This occurred in MPCs at both early and late stages of myogenic commitment. In fact, early MPCs isolated from 6-week-old dKO mice have reductions in proliferation, resistance to oxidative stress and multilineage differentiation capacities compared with age-matched *mdx* MPCs. This effect may potentially be mediated by fibroblast growth factor overexpression and/or a reduction in telomerase activity. Our results demonstrate that the rapid disease progression in the dKO model is associated, at least in part, with MPC depletion. Therefore, alleviating MPC depletion could represent an approach to delay the onset of the histopathologies associated with DMD patients.

INTRODUCTION

Duchenne muscular dystrophy (DMD), an X-linked progressive muscle wasting disease, is caused by a deficiency in dystrophin, a cytoskeletal protein that is essential for the membrane stability of the multinucleated myofibers of skeletal muscle (1). DMD is the most common form of muscular dystrophy, occurring in ~1 of every 3300 boys (2). In DMD patients, the loss of sarcolemmal dystrophin promotes damage during muscle contraction (3–7). This process results in an efflux of creatine kinase (CK), an influx of calcium ions and the recruitment of T cells, macrophages and mast cells to the damaged muscle, leading to progressive myofiber necrosis, fibrosis and muscle weakness (8). Patients typically lose the ability to independently ambulate by the middle of their second decade of life. Death, due to cardiac or respiratory failure, typically occurs during their third decade (9).

Normally, skeletal muscle possesses a robust regenerative capacity due to the presence of adult muscle progenitor cells (MPCs), which play an important role in postnatal muscle growth and repair. Many cell populations with myogenic potential have been reported; however, their origin and relationship to each other remain unclear. Satellite cells, which are located between the basal lamina and the muscle fiber plasma membrane (10), were first defined as the major source of MPCs that regulates postnatal skeletal muscle growth and regeneration (10–13). Other myogenic progenitors, such as bone marrow-derived circulating stem cells, various cell populations residing in the muscle interstitium (14–17) and blood vessel walls (18–20), have also been identified as potential cell sources for muscle repair (21). Following engraftment into damaged or diseased muscle, these non-satellite cell progenitors are capable of adopting a skeletal myogenic fate (22). Researchers have isolated MPCs utilizing a variety of methods, including cell culture selection techniques, flow cytometry-based sorting using cell surface markers and Hoechst dye exclusion (23–28). Our research group has reported the isolation of muscle-derived stem cells (MDSCs) based on their adhesion characteristics, through the use of the preplate technique (29). MDSCs are capable of undergoing multilineage

*To whom correspondence should be addressed at: Department of Orthopaedic Surgery, University of Pittsburgh, Pittsburgh, Bridgeside Point 2, 450 Technology Dr. Pittsburgh, PA, 15219, USA. Tel: +1 4126482641; Fax: +1 4126484066; Email: jhuard@pitt.edu

© *The Author 2014. Published by Oxford University Press. All rights reserved.*
For Permissions, please email: journals.permissions@oup.com

differentiation (26,30–32) and have been shown to be superior to myoblasts for muscle regeneration (29). Myoblasts are committed to the myogenic lineage (late muscle progenitors) and readily fuse together or with injured mature myofibers to regenerate injured muscle.

In DMD, recurrent myofiber damage elicits a constant need for repair, thus giving way to the depletion of the MPC pool and the loss of functional muscle regeneration. Eventually, muscle is replaced by fibrotic tissue, calcium deposits and adipose tissue, which plays a critical role in the wasting process observed in DMD (33). Interestingly, it has been reported that the dystrophin mutation associated with *mdx* mice does not directly impair satellite cell function, suggesting that the failure of effective repair is a likely consequence of a cascade of pathological damage (34). Notably, despite the lack of dystrophin at birth, the onset of muscle weakness in DMD patients does not occur until 3–5 years of age, coinciding with the depletion of the MPC pools. Previous studies have shown that myoblasts isolated from DMD patients are impaired and exhibit a severe proliferation deficit *in vitro,* which becomes more pronounced as patients age (35,36); hence, we can theorize that DMD represents a form of accelerated aging that presents primarily in skeletal muscle.

The *mdx* mouse is the most widely used animal model of DMD, and like DMD patients, lacks dystrophin due to a point mutation in the dystrophin gene (9,37,38). However, in contrast to DMD patients, these mice only exhibit a mild dystrophic phenotype. In fact, these mice often live up to 2 years of age, comparable to the lifespan of normal, wild-type (WT) mice. Furthermore, *mdx* mice do not exhibit the rapid loss of muscle strength and early death observed in DMD patients (39,40). Additionally, various clinical features typical of DMD patients, such as pseudohypertrophy, scoliosis and cardiomyopathy, are not observed in young *mdx* mice (41–43). Although the exact reason why *mdx* mice do not recapitulate the human DMD phenotype is still unclear, it has been suggested that *mdx* mice compensate for the lack of dystrophin by upregulating utrophin, a protein structurally similar to dystrophin (44–46). Under homeostatic conditions, utrophin localizes to the sarcolemma of skeletal muscle fibers during fetal development, but is replaced by dystrophin at the myofiber sarcolemma after birth, and only continues to persist at neuromuscular and myotendinous junctions (NMJ and MTJ) (47,48). Utrophin expression around the sarcolemma of regenerating myofibers in adult *mdx* skeletal muscle is believed to compensate for dystrophin deficiency (45,46,49). Supporting this hypothesis, previous studies have reported that dystrophin and utrophin double knock-out (dKO) mice (*dystrophin*$^{-/-}$/*utrophin*$^{-/-}$) share many more histopathological symptoms with DMD patients than do *mdx* mice (50,51).

In this study, we tested the hypothesis that the rapid progression of muscular dystrophy in DMD patients is associated with a rapid depletion of MPCs. In support of this contention, it has been recently reported that shortening the telomeres of muscle cells in *mdx* mice by muscle-specific deletion of the RNA component telomerase, results in mice (*mdx*/mTR) with a much more severe dystrophic phenotype that progressively worsens with age (52).

For our investigation, we compared the dKO and *mdx* mouse models in order to further investigate whether the rapid disease progression observed in dKO mice is associated, at least in part, with a depletion of MPCs. our results indicated that dKO mice have a much more severe phenotype than *mdx* mice, including the intramuscular accumulation of necrosis and fibrosis, as well as calcium deposits. Following weaning, dKO mice experience weight loss, progressive loss of muscle force, kyphosis and a shortened lifespan, consistent with the animal model previously described (50,51). Importantly, we show here that the severity of the dKO phenotype progressively worsens with age and is associated with the depletion of MPCs, including both early and late myogenic progenitors (MDSCs, satellite cells and myoblasts) (29,53). In addition, we also observed increased expression of fibroblast growth factor 2 (FGF2) and decreased telomerase activity in the muscles of the dKO mice compared with muscles of age-matched *mdx* mice. These results suggest that high FGF2 expression may promote a decline in stem cell number and function during disease progression, and insufficient telomerase activity may result in progressive telomere shortening, ultimately leading to cellular senescence. This finding supports our hypothesis that the pathology associated with the dKO phenotype is initiated by both dystrophin and utrophin deficiency, but rapidly progresses and increases in severity because of stem cell depletion. Taken together, these observations suggest that preventing the depletion of the MPC pools could be a novel approach to delay the histopathologic symptoms associated with the skeletal muscles of DMD patients.

RESULTS

Severe muscle histopathology in dKO mice

Mdx mice do not show any significant muscle pathology until 3–4 weeks after birth, when the onset of necrosis is first seen in the diaphragm muscle. To determine the age of onset of muscular dystrophy in the dKO mice, the gastrocnemius and diaphragm muscles from 5-day-old dKO mice were examined and compared with muscles from *mdx* littermates. Hematoxylin and eosin (H&E) staining revealed that dKO muscle histopathology started as early as 5 days of age, as evidenced by extensive cell infiltration in both the diaphragm and gastrocnemius muscles (Supplementary Material, Fig. S1). Many necrotic fibers were seen in the 5-day-old dKO diaphragm, but not in the age-matched *mdx* littermates (data not shown). To characterize the progression of the dystrophic histopathology, the gastrocnemius and diaphragm muscles of 6- to 8-week-old dKO mice were analyzed and compared with that of age-matched *mdx* and WT mice. Much larger areas of myofiber necrosis, massive cellular infiltration and connective tissue deposition were seen in the gastrocnemius muscles of the dKO mice compared with the WT and *mdx* mice (Fig. 1A). Mouse IgG-positive necrotic fibers were markedly increased in the dKO gastrocnemius muscles compared with the *mdx* and WT muscles (Fig. 1B, Supplementary Material, Fig. S3B). Aggregates of calcium deposition (Fig. 1C) and fibrosis (Fig. 1D, Supplementary Material, Fig. S3C) were also substantially increased in the dKO muscles. We observed a similar histopathology in the diaphragm muscles of dKO mice (Supplementary Material, Fig. S2). Together, these results demonstrate that, in contrast to age-matched WT and *mdx* mice, the dKO mice rapidly developed a muscle histopathologic phenotype similar to DMD patients.

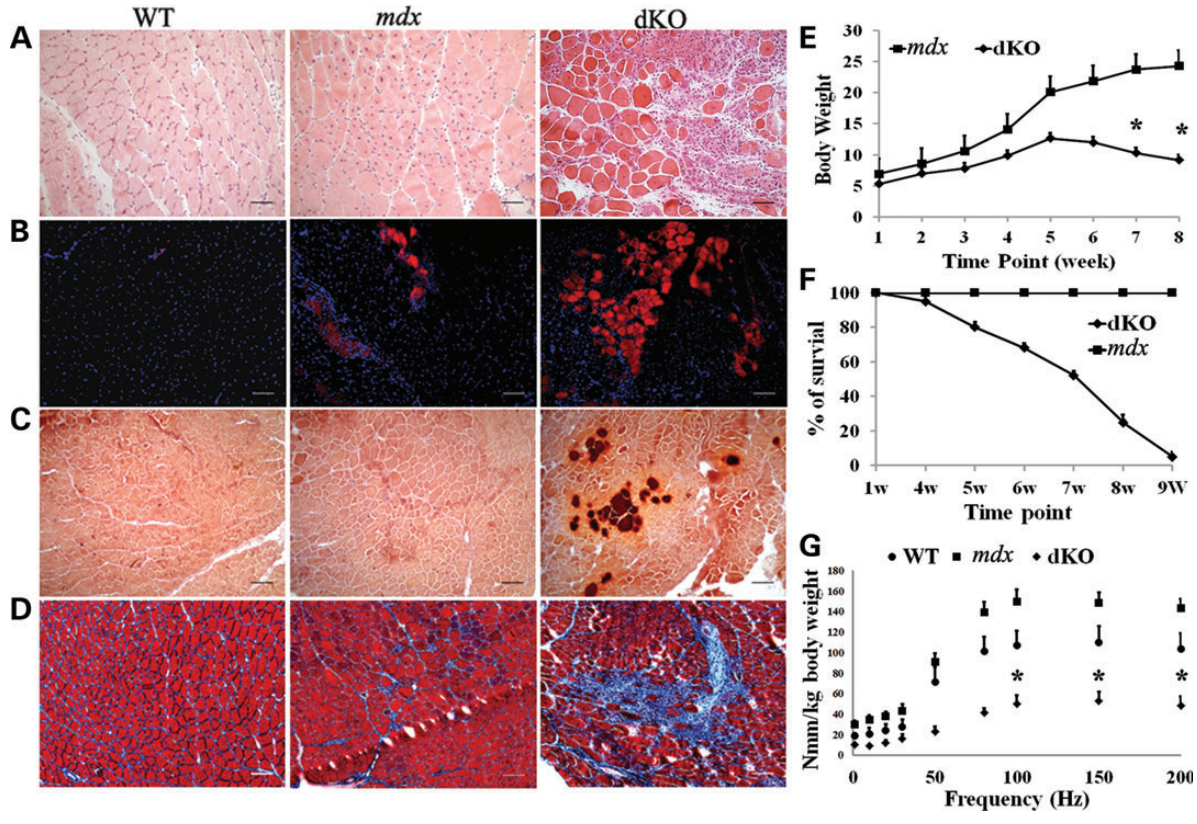

Figure 1. Muscle histopathology and dystrophy are more severe in the dKO mice compared with the WT and *mdx* mice. (**A**) H&E staining shows severe muscle damage in the gastrocnemius muscle of 8-week-old dKO mice. These fibers have fewer centrally nucleated fibers compared with age-matched WT and *mdx* muscles. (**B**) Necrotic areas in the gastrocnemius muscles were identified by mouse IgG staining. (**C**) Alizarin red staining to visualize calcium deposits in 8-week-old WT, *mdx* and dKO muscles. (**D**) Trichrome staining of muscle sections to identify fibrotic regions. (**E**) The body weight of the dKO mice significantly decreased after 5–6 weeks of age. Error bars indicate 'mean ± SD', $n = 10$. $^*P < 0.01$. (**F**) dKO mice have a significantly shorter lifespan than WT and *mdx* mice. Error bars indicate 'mean ± SD', $n = 30$. (**G**) The results from muscle physiology testing showed a significant decrease in muscle strength in the dKO mice, $n = 6$. Error bars indicate 'mean ± SD', $^*P < 0.05$. In (A),' all scale bars = 50 μm; in (B–D), all scale bars = 100 μm.

Given the important physiological differences between the diaphragm and gastrocnemius muscles, we compared the histopathology of these two muscles in dKO and *mdx* mice. We found that the diaphragms from both dKO and *mdx* mice exhibited progressive muscle degeneration. The percentage of centrally nucleated fibers was 2-fold greater in the gastrocnemius compared with the diaphragm muscles **(**Supplementary Material, Fig. S3A**)**, consistent with the impaired regeneration of the diaphragm muscles observed by other groups (54). Most notably, diaphragm muscles from dKO mice at 6–8 weeks of age had extensive fibrosis (Supplementary Material, Figs S2 and S3C**)**, but less necrosis when compared with age-matched *mdx* mice (Supplementary Material, Figs S2 and S3B), suggesting a more rapid progression of the disease in the dKO mice. We also observed less calcium deposition (data not shown) in the diaphragm compared with gastrocnemius muscles of dKO mice.

The dKO mice also rapidly developed marked kyphosis, weight loss (Fig. 1E) and shortened lifespan (Fig. 1**F**). These mice began to die at 4–6 weeks of age, and very few lived up to 9 weeks of age. In contrast, most *mdx* mice do not show a lifespan difference compared with normal WT animals. To assess muscle performance, we next measured the isometric torque of the anterior crural muscles in 6- to 8-week-old mice. Our results indicated that muscle function significantly decreased in the dKO mice, compared with age-matched WT and *mdx* mice (Fig. 1G). In order to account for the smaller size of the dKO mice, muscle function was normalized to body weight. This result provides direct evidence of severe muscle weakness in the dKO mice. In contrast, the function of the anterior crural muscles from *mdx* mice was greater than that of the muscles from the WT control mice, which is consistent with a previous study that showed that young *mdx* mice have higher muscle mass and greater muscle function compared with age-matched WT mice (6).

MPCs from dKO skeletal muscles are depleted

To test whether the skeletal muscle damage observed in dKO mice was associated with MPC depletion, MPCs were isolated from the limb muscles of 5-day-old and 6- to 8-week-old dKO, *mdx* and WT mice. Following a series of enzymatic digestions, the muscle cells were seeded on collagen type I-coated flasks. The next day, floating cells, which included most of the myogenic cells, were labeled with antibodies against CD34, Sca-1 and CD45, and subsequently analyzed by flow cytometry. The CD34+/Sca-1−/CD45− cells were classified as MPCs (55). Our results demonstrated that the percentage of CD34+/Sca-1−/CD45− cells isolated from 5-day-old dKO mice

(2.2%) was similar to that from age-matched *mdx* littermates (1.9%) (Supplementary Material, Fig. S4A), indicating that there was no difference in the initial number of CD34+/Sca-1−/CD45− cells between the dKO and *mdx* mice during the first few days after birth. After 5–7 weeks, however, the number of MPCs present in the dKO mice significantly declined when compared with age-matched *mdx* and WT mice (Fig. 2A and B). Finally, the myogenic potential of the CD34+/Sca-1−/CD45− cell fractions were further confirmed by their ability to differentiate into myotubes (Fig. 2C).

Pax7-positive muscle satellite cells represent a population of myogenic progenitors responsible for postnatal growth, repair and maintenance of skeletal muscle. We hypothesized that the muscle satellite cell pool might also change in the dKO muscle during the disease progression. To test this possibility, we first analyzed the number of Pax7-positive cells that were present in the diaphragm and gastrocnemius muscles of these mice at 5 days of age. We found that the gastrocnemius of the dKO mice possessed the same number of Pax7-positive cells as observed in *mdx* mice; however, in the diaphragm, more Pax7-positive satellite cells were seen in the dKO mice than in the *mdx* mice (Supplementary Material, Fig. S4B). This corresponds to the degenerative changes observed in the dKO mice, as early as 5 days of age, indicating that their satellite cells are activated and proliferating. To assess whether the disease progression was related to a decline in the number of satellite cells, the diaphragm muscles from these mice were next evaluated at 8 weeks of age. We observed, at this time, that the number of Pax7-positive cells were markedly reduced in the dKO mice (Fig. 2D and E) when compared with age-matched *mdx* and WT mice. Moreover, the results from real-time polymerase chain reaction (PCR) confirmed that there was a rapid and significant decline in Pax7 mRNA in the diaphragm muscles of dKO mice isolated from 4- to 8-week-old mice when compared with that observed in the *mdx* and WT diaphragm muscles (Fig. 2F). Taken together, our results demonstrated that MPCs, including CD34+/Sca-1−/CD45− cells and Pax7-positive satellite cells, underwent a rapid decline in the skeletal muscles of dKO mice during the progression of the disease. These data confirm that the skeletal muscle of 6- to 8-week-old dKO mice becomes more severely affected than *mdx* muscle, highlighting the fact that a reduction in the number of MPCs correlates with the severity of the dKO phenotype.

Impaired proliferation and differentiation of MPCs isolated from dKO single muscle fibers

To determine whether there was also a reduction in MPC proliferation and differentiation potentials, we assessed the myogenic potential of cells derived from dKO single muscle fiber isolations performed on the EDL muscles of 6- to 8-week-old animals. First, we observed more damaged muscle fibers in the dKO muscles ($53 \pm 12\%$) compared with the *mdx* muscles ($34 \pm 8\%$) 24 h after the single fibers attached to the matrigel-coated plates (Fig. 3A). The proliferative potential of the MPCs migrating from the isolated myofibers was analyzed after 4 days of culture. These satellite cell-derived cells were immunostained for desmin, an established myogenic marker. We observed that the number of desmin-positive cells emanating from the single fibers was significantly decreased in dKO mice compared with *mdx* mice (Fig. 3B and C), indicating that the MPCs derived from the single myofibers of dKO muscle exhibited a reduced proliferative potential compared with the *mdx* MPCs. In addition, at 7 days post culturing, immunostaining for fast myosin heavy chain (MyHCf), a terminal myogenic differentiation marker, was performed to determine the myogenic differentiation capacity of the MPCs. We observed that the MPCs released from the *mdx* muscle fibers formed more MyHCf+ multinucleated myotubes than those migrating from the dKO muscle fibers (Fig. 3D, E and F). These results support both a reduction in the proliferation and differentiation potentials of the MPCs derived from the dKO mice. The data shown here provide more evidence to suggest that defective proliferation and differentiation capacities of the MPCs in the dKO mice leads to a reduction in muscle repair, which is similar to what is observed in DMD patients (35).

The function of myoblasts is also impaired in dKO mice

Next, we asked whether myoblast dysfunction could also be observed in dKO mice. Utilizing the previously described preplate technique, we isolated many populations of MPCs, including myoblasts, from 6-week-old WT, *mdx* and dKO mice. We observed that the number of preplate (PP) 5 and PP6 cell populations, which contain muscle stem cells (29,56), was decreased in the muscles of dKO mice (Fig. 4A). We further tested the rapidly adhering cell populations (PP3 and PP4), which contain mostly satellite cell-derived myoblasts (29,56), for their differentiation capacity *in vitro*. PP3 and PP4 cells were cultured in proliferation medium until the cells reached 80% confluence, at which point the culture medium was changed to differentiation medium (2% FBS). Three days later, immunofluorescent staining for fast skeletal myosin heavy chain was performed. In comparison to the PP3 and PP4 cells from WT and *mdx* mice, which formed numerous, large multinucleated myotubes, the PP3 and PP4 populations isolated from the dKO mice formed fewer and smaller myotubes (Fig. 4B), which indicates the myogenic differentiation potential of the dKO myoblasts is also significantly reduced relative to the *mdx* and WT myoblasts ($P < 0.05$) (Fig. 4C). This result demonstrated that myoblasts isolated from dKO mice are also impaired in their differentiation capacity, which is similar to what is observed in myoblasts isolated from DMD patients.

The function of muscle-derived stem cells isolated from dKO mice is defective

We next assessed the characteristics of the slowly adhering fraction of cells isolated from the skeletal muscles of dKO, *mdx* and WT, which contains a heterogeneous population of stem and progenitor cells that we refer to as muscle-derived stem cells (MDSCs) (29,53). MDSCs display unique characteristics that are associated with non-committed progenitor cells. For example, we have previously shown that MDSCs express markers associated with stem cells and are capable of self-renewal *in vitro* (29). Furthermore, MDSCs have been shown to be capable of replenishing the MPC pool when injected into dystrophic murine muscle and contribute to the persistent restoration of dystrophin (29,57). We isolated MDSCs from 6- to 8-week-old dKO, *mdx* and WT mice and examined their function

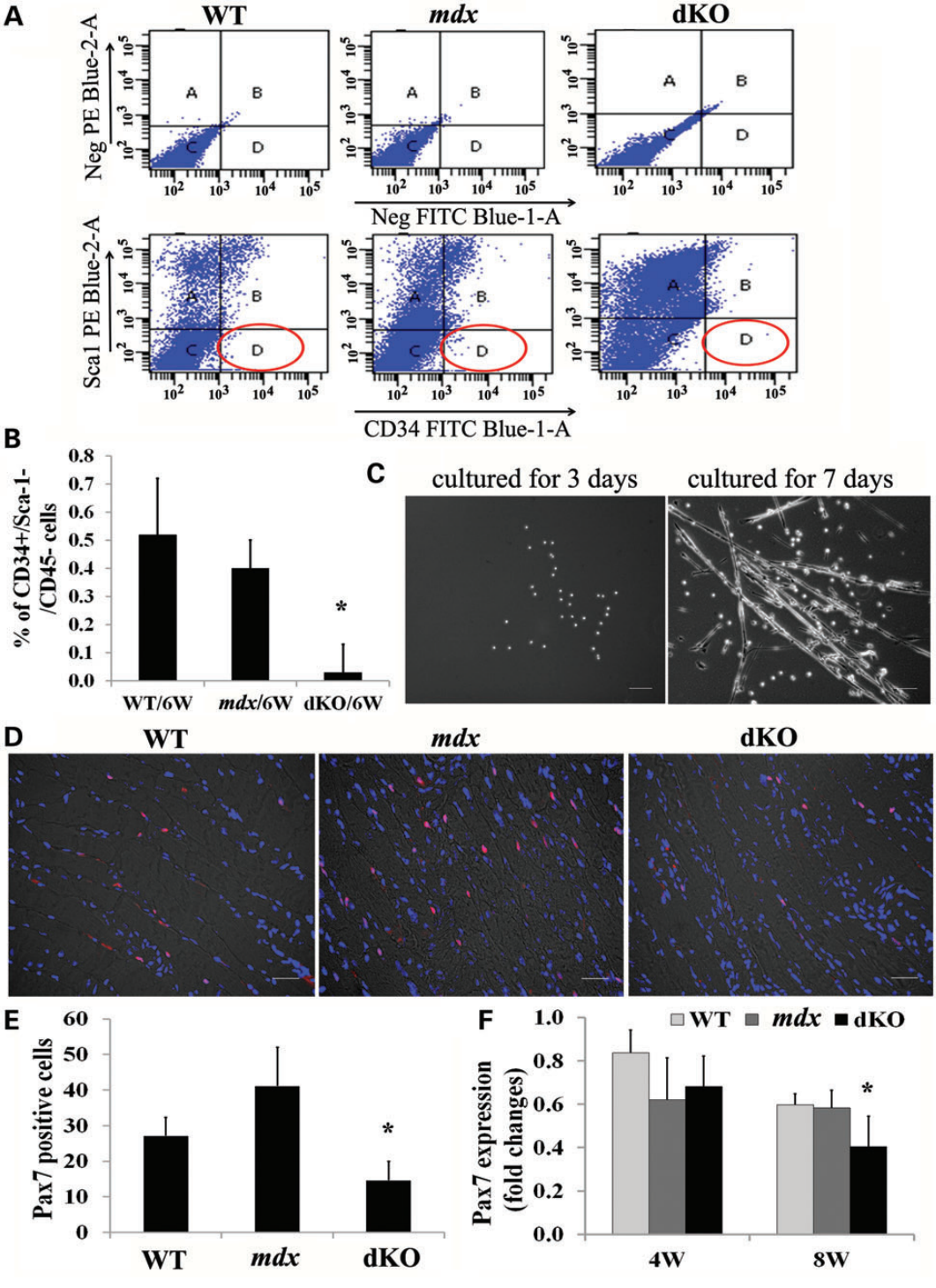

Figure 2. The muscle progenitor cell pool is exhausted in old dKO mice. (**A**) Fluorescence activated cell sorting (FACS) plots show that almost no CD34+/Sca-1− cells could be detected in 6-week-old dKO muscles. (**B**) Quantification of FACs results. Error bars indicate 'mean ± SD,' $n = 3$, $^*P < 0.01$. (**C**) CD34+/Sca-1−/CD45− cells from *mdx* mice were cultured for 3 and 7 days, multinucleated myotubes were monitored using bright field microscopy. (**D**) Diaphragmatic cryosections from 8-week-old dKO, *mdx* and WT mice were immunostained for the myogenic progenitor cell marker Pax7. (**E**) Quantitation of Pax7-positive cells in the diaphragm muscles of 8-week-old mice. The Pax7-positive cells were quantified based on the total number of Pax7-positive cells in each 200× image (the data represent 3 mice/group). Error bars indicate 'mean ± SD'. $^*P < 0.01$. (**F**) Graph showing the results of real-time PCR. RNA was isolated from three diaphragms of each genotype. Error bars indicate 'mean ± SD'. $^*P < 0.05$. In (C), all scale bars = 100 μm and in (D), all scale bars = 25 μm.

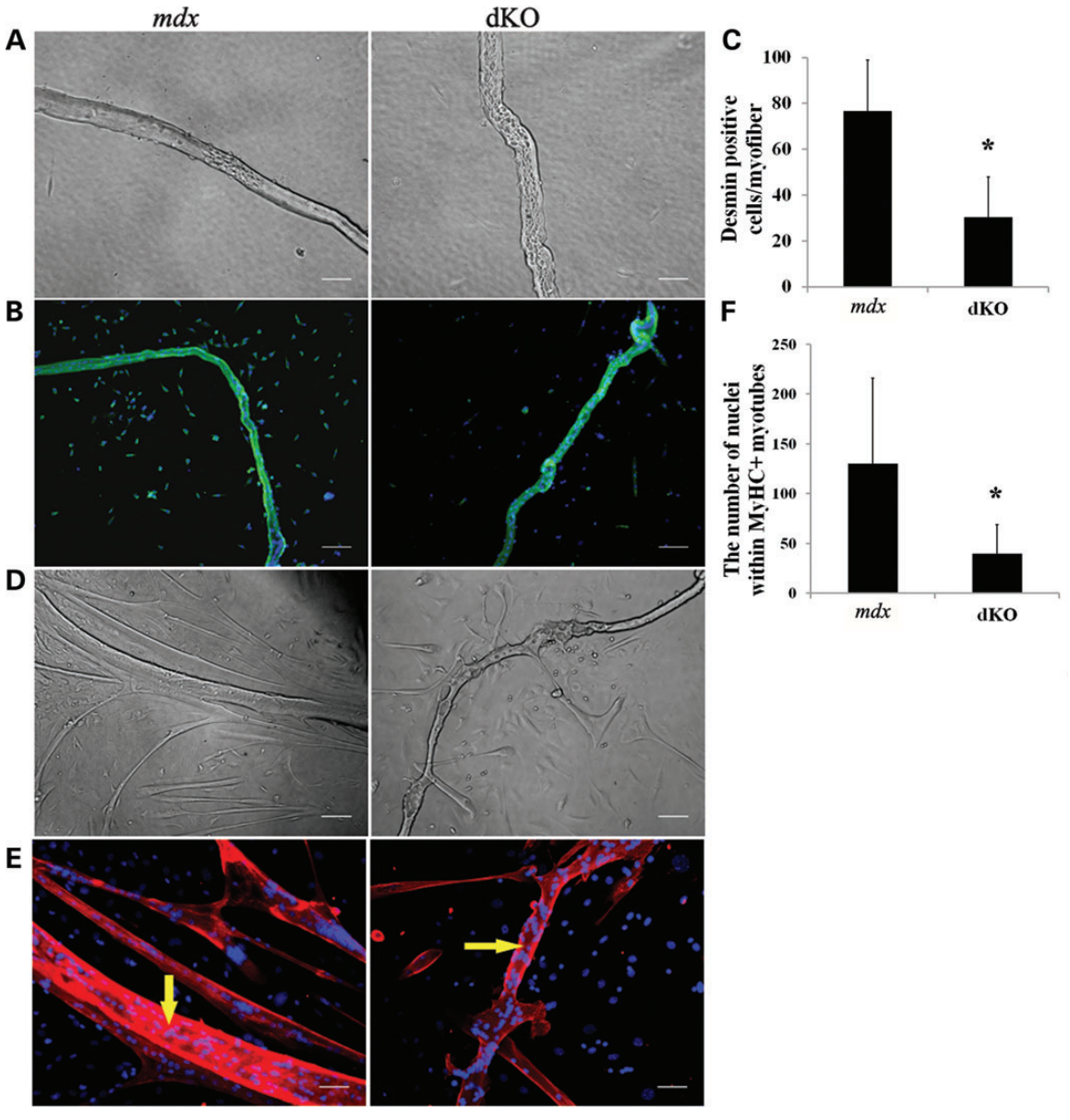

Figure 3. MPCs from single-muscle fibers isolated from dKO mice exhibit proliferation and differentiation defects. (**A**) Single-muscle fibers isolated from 6- to 8-week-old mice. Abnormal single muscle fibers are shown in bright field. (**B**) Desmin was stained after 96 h of culture (green cells). Representative images show a proliferation defect in the dKO muscles compared with *mdx* muscles. (**C**) Quantification of desmin-positive cells derived per fiber, the muscle fibers were isolated from three EDL muscles of each genotype. Error bars indicate 'mean ± SD', $^{*}P < 0.01$. (**D**) Single-muscle fibers were cultured for 7 days. Representative images showing myotube formation in both dKO and *mdx* fiber cultures (bright field). (**E**) Representative images of immunofluorescent staining for fast myosin heavy chain (MyHCf) (red) and nuclei (blue) indicated myogenic differentiation. Yellow arrows show the original myofibers. (**F**) Graph showing quantification of the differentiation capacity as the total number of nuclei in MyHCf-positive myotubes derived per muscle fiber after 7 days of culture. $n = 5$. $^{*}P < 0.05$. In (A) and (E), all scale bars = 50 μm, and in (B) and (D), all scale bars = 100 μm.

by measuring relative differences in their capacities for proliferation, myogenic differentiation, resistance to oxidative stress and also multiple lineage differentiation. To examine the proliferation kinetics of cell populations *in vitro*, we used the LCI system described above (58) and observed a significant reduction in the proliferation capacity of the dKO MDSCs when compared with the *mdx* and WT MDSCs (Fig. 5A). Next, to compare the myogenic differentiation capacity of the MDSCs isolated from dKO, *mdx* and WT mice *in vitro*, equal numbers of cells from each group were plated in 24-well plates and switched to differentiation medium once the cells adhered. After 3 days, the majority of the WT (69%) and *mdx* cells (80%) had differentiated into myotubes, as determined by immunodetection of MyHCf (Fig. 5B). The differentiation potential of the dKO MDSCs was observed to be significantly lower ($P < 0.01$; Fig. 5C). We next examined cellular resistance to hydrogen peroxide-induced oxidative stress. Each of the populations (dKO, *mdx* and WT) was exposed to 400 μM hydrogen peroxide in proliferation medium containing PI, and the LCI system was used to identify the number of PI+ cells in order to determine

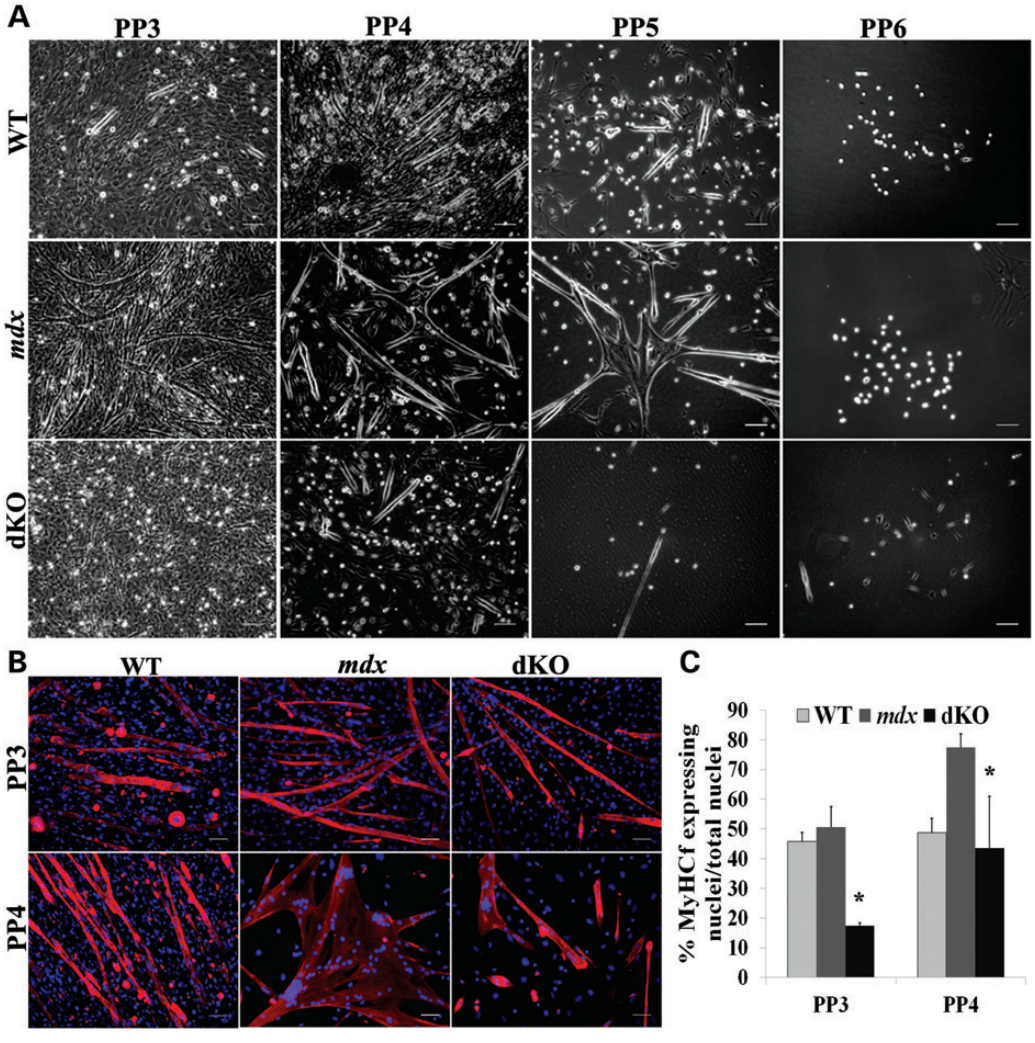

Figure 4. dKO muscle progenitor cells are impaired in their differentiation capacity. (**A**) Various populations of muscle-derived cells were isolated according to their adhesion characteristics by the preplate technique. Representative images showing different MPC populations isolated from WT, *mdx* and dKO mice. (**B**) Representative images of PP3 and PP4 cell populations isolated from WT, *mdx* and dKO mice at 6 weeks of age and immunostained for MyHCf (red) and DAPI (blue). (**C**) Graph showing quantification of the cells differentiation capacity as the number of nuclei in MyHCf-positive myotubes relative to the total number of nuclei. $n = 5$. Error bars indicate 'mean $\pm$ SD'. $^{*}P < 0.05$. In (A), all scale bars = 100 μm, and in (B), all scale bars = 50 μm.

the percentage of cell death. In comparison with the *mdx* and WT MDSCs, the dKO MDSCs displayed a significant reduction in their resistance to oxidative stress ($^{*}P < 0.05$, Fig. 5D). Of note, we found that dKO MDSCs isolated from 5-day-old mice demonstrated similar a proliferation rate and myogenic differentiation capacity as seen in age-matched WT MDSCs (data not shown), which suggests that stem cell function rapidly declines in the dKO MDSCs from 5 days to 6–8 weeks of age (Supplementary Material, Fig. S4C and D). Finally, we examined the dKO, *mdx* and WT MDSC capacity for multilineage differentiation. Our results indicated that there was a reduction in the adipogenic, osteogenic and chondrogenic differentiation capacities of the MDSCs isolated from the dKO mice compared with the MDSCs isolated from the *mdx* and WT mice (Fig. 5E). Together, these data suggest that, when compared with WT and *mdx* MDSCs, the functionality of aged dKO MDSCs was severely affected.

Impaired muscle regeneration potential of MPCs in dKO mice

We next examined *in vivo* muscle regeneration and inflammation by assessing embryonic myosin heavy chain (eMyHC) and F4/80 (macrophage marker) expression in young (4 weeks) and old (6–8 weeks) dKO muscle. eMyHC is expressed almost exclusively in newly regenerating muscle fibers, which is usually found after acute muscle injury or in a disease state. eMyHC is typically expressed for ~1 week within the newly regenerated muscle fibers. Normally, during the regenerative phase of *mdx* muscle pathology, eMyHC-positive fibers are surrounded by F4/80-positive macrophages. The gastrocnemius muscle sections from 4–week-old and 6- to 8-week-old dKO mice were examined for eMyHC and F4/80 expression. We observed that the number of eMyHC-positive fibers (green) significantly declined in the dKO muscles from 4 to 8 weeks (Fig. 6A and B), but macrophage

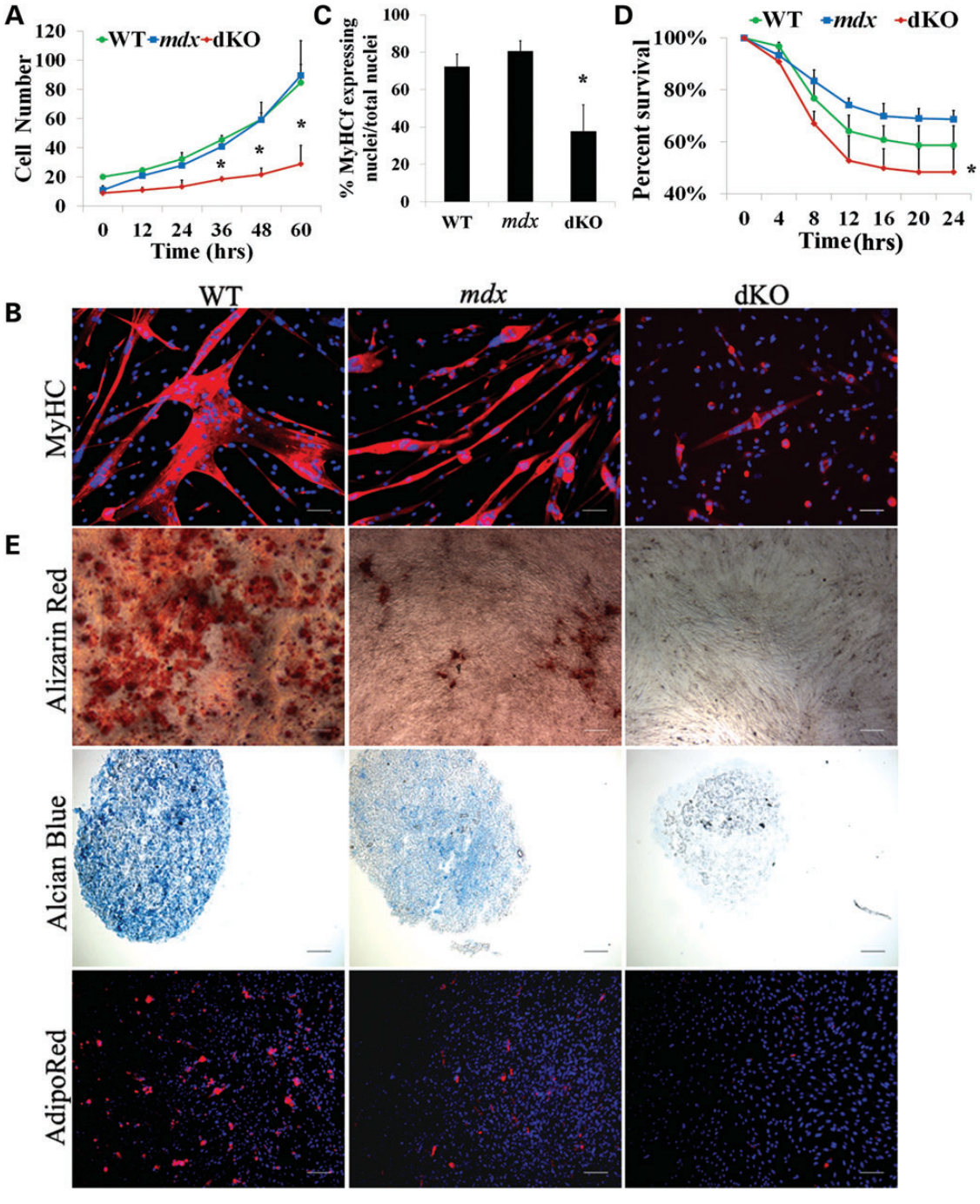

Figure 5. Muscle-derived stem cells (MDSCs) isolated from aged dKO muscle exhibit a reduction of their functionality. (**A**) Cell proliferation rate was measured using a Live Cell Imaging (LCI) system. The graph displays the average number of cells at each time point (calculated from 3–4 populations per genotype). Error bars indicate 'mean ± SD'. $^*P < 0.01$. (**B**) MDSCs were cultured in myogenic differentiation medium for 3 days. Cell fusion into multinucleated myotubes was determined by immunostaining for MyHCf, a terminal myogenic differentiation marker. (**C**) Myogenic differentiation was quantified by calculating the number of nuclei in MyHCf-positive myotubes relative to the total number of nuclei in the culture. A total of three populations of WT, *mdx* and dKO MDSCs were tested. Error bars indicate 'mean ± SD'. $^*P < 0.01$ (**D**) Each cell population (dKO, *mdx* and WT) was exposed to 400 μM hydrogen peroxide in proliferation medium containing PI. Using the LCI system, 100× bright field and fluorescence images were taken at 10 min intervals over 24 h. Identifying the number of PI+ cells per field of view out of the total cell number determined the percentage of cell death over time. Error bars indicate 'mean ± SD', $n = 3$, $^*P < 0.01$. (**E**) Multilineage differentiation of MDSCs. The three populations of cells were cultured in insulin mediated adipogenic differentiation medium, BMP2 supplemented osteogenic medium and chondrogenic induction media supplemented with BMP2 and TGFβ3, respectively, and then alizarin red (top), alcian blue (middle) and AdipoRed (bottom) staining were performed. In (B), all scale bars = 50 μm. In (E), scale bar = 50 μm for alizarin red and alcian blue, scale bar = 100 μm for AdipoRed.

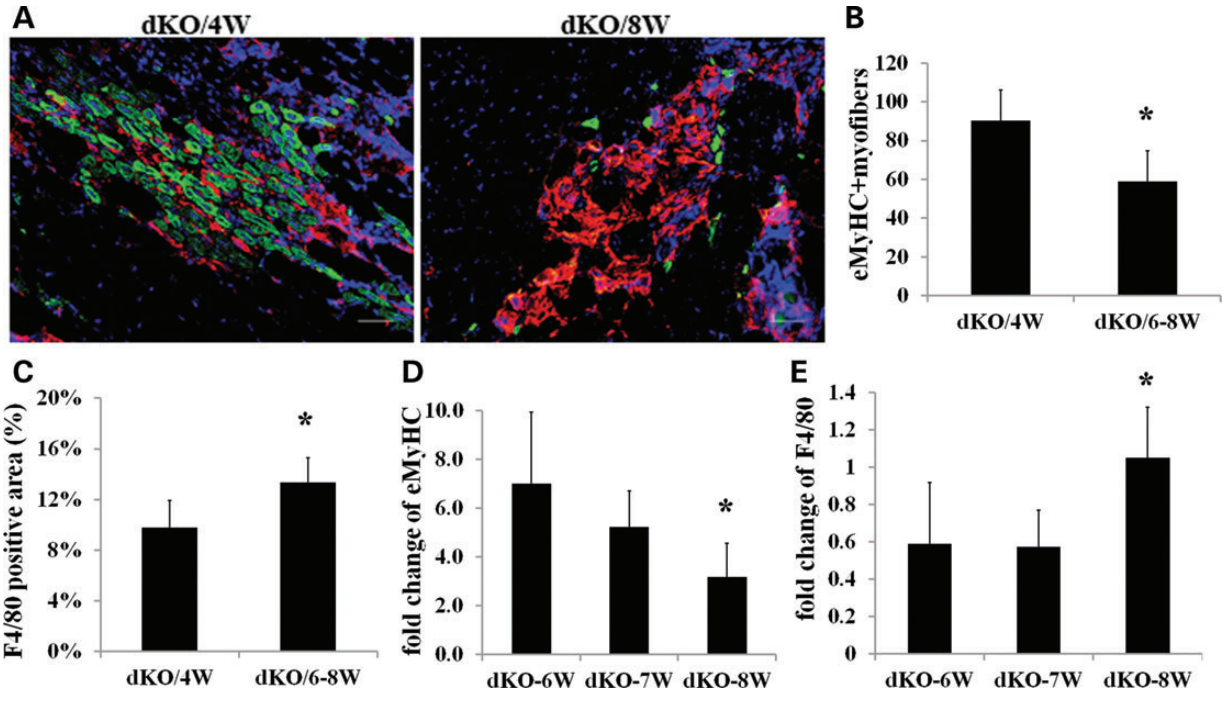

Figure 6. Limited muscle regeneration potential of MPCs in dKO mice *in vivo*. (**A**) Representative images showing cryosections from young (4 weeks old) and old (6–8 weeks old) dKO gastrocnemius muscles stained for eMyHC (green) and F4/80 (red). Scale bars = 50 μm. (**B**) Graph showing quantification of eMyHC-positive fibers, $n = 5$, error bars indicate 'mean ± SD', $^*P < 0.05$. (**C**) Graph showing quantification of F4/80-positive macrophages. Macrophage infiltration areas in the gastrocnemius muscles were quantified based on the total positive area per image (the data represent 5 muscles per group). $^*P < 0.05$. (**D**) Graph showing the results of real-time PCR for eMyHC expression. RNA was isolated from 3–6 gastrocnemius muscles from dKO mice. (**E**) Graph showing the results of real-time PCR for F4/80 expression. RNA was isolated from 3–6 gastrocnemius muscles from dKO mice. Error bars indicate 'mean ± SD'. $^*P < 0.05$.

infiltration (red) increased with age and correlated with the progression of the disease state (Fig. 6A and C). Similarly, real-time PCR for F4/80 and eMyHC from 6- to 8–week-old dKO mice demonstrated that the level of inflammation (F4/80 gene expression) increased, whereas muscle regeneration (eMyHC expression) decreased during the progression of the disease from 6 to 8 weeks (Fig. 6D and E). These data indicate that dKO MPCs have a reduced ability to efficiently regenerate new myofibers as they age, a process likely related to the increase in inflammation over time.

Higher FGF2 expression in dKO skeletal muscle

The above data have provided strong evidence suggesting that the progression of muscular dystrophy in dKO mice is associated with rapid MPC depletion, similar to that seen in DMD patients (35); however, the mechanism responsible for this phenomenon is still unclear. A study from a recent paper demonstrated that increased FGF2 signaling is a major contributor to the loss of stem cell quiescence and possibly even stem cell depletion during aging under homeostatic conditions (59). We questioned whether FGF2 may be a contributing factor involved in the depletion of MPCs in dKO mice. Therefore, FGF2 expression was examined in dKO and age-matched *mdx* muscle tissue sections. Strikingly, FGF2 expression was observed in dKO muscle as early as 6 weeks, whereas FGF2 was not detected in *mdx* muscle until 24 months of age (Fig. 7A). Real-time PCR confirmed this observation (Fig. 7B). These results indicate that increased FGF2 signaling may play a role in the decline of resident MPCs, eventually diminishing the regenerative capacity of the skeletal muscle.

Lower telomerase activity in muscle-derived stem cells isolated from dKO mice

In addition, recent studies have reported that the impaired replicative potential of myoblasts from DMD patients is related, at least in part, to telomere shortening, a common feature of dystrophic human muscle cells with increasing age (60). Indeed, it has also been reported that both muscle stem cell exhaustion and cell senescence could be a result of impaired telomerase activity (52,61,62). Therefore, we assessed telomerase activity in MDSCs isolated from *mdx* and dKO mice using the Telomerase PCR ELISA kit. In comparison with age-matched *mdx* MDSCs (4 weeks of age), the telomerase activity of the dKO MDSCs was significantly reduced (Fig. 7C). These results suggest that the decreased telomerase activity observed in the dKO MDSCs may play a major role in the rapid progression of the muscle histopathology in dKO mice, when compared with age-matched *mdx* MDSCs.

DISCUSSION

Although various mouse models for DMD have been investigated, we are still lacking a reliable mouse model that faithfully mimics the DMD pathology, which could consequently be used to test potential therapies. *Mdx* mice are the most widely used animal model of DMD because they are deficient in dystrophin;

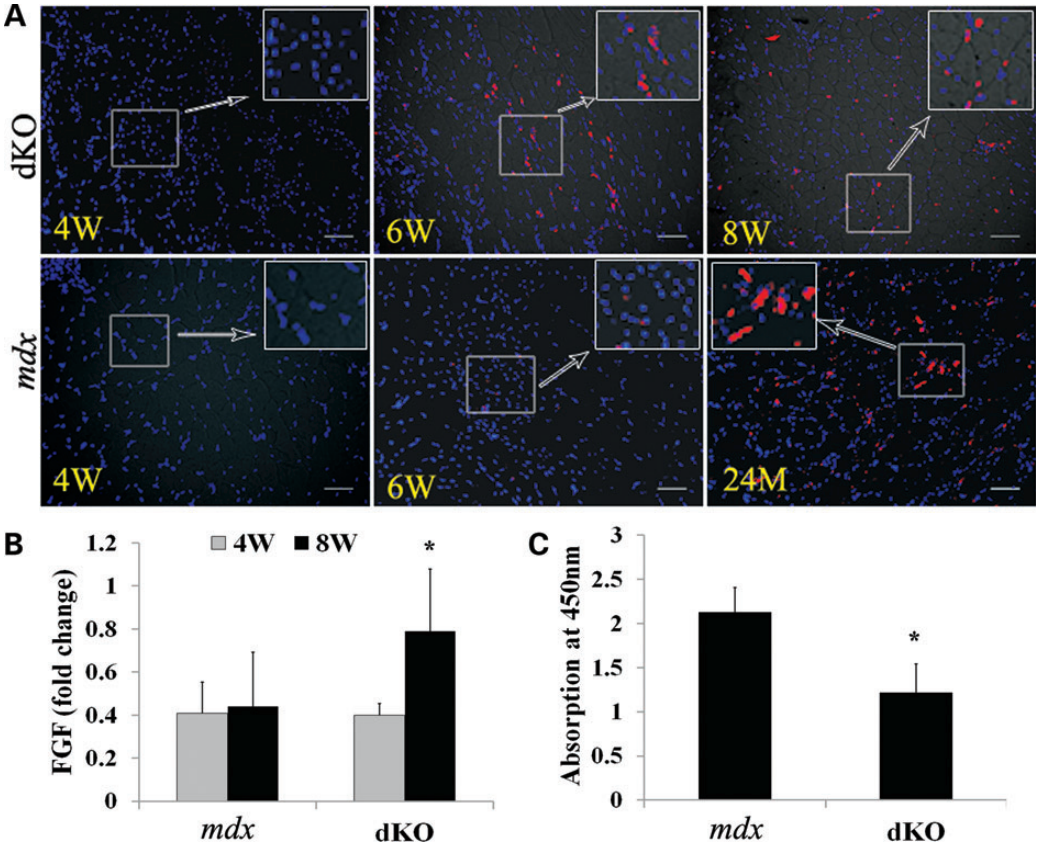

Figure 7. Increased FGF2 expression and lower telomerase activity were detected in dKO mice. (**A**) Representative images of immunofluorescent staining for FGF2 expression of dKO and *mdx* muscles (red cells) at different ages. (**B**) RNA was extracted from frozen muscle tissue and real-time PCR was performed. The graph shows the quantification of the PCR results ($^*P < 0.05$). (**C**) Telomerase activity in the MDSCs was detected with TeloTAGGG Telomerase PCR ELISA kit. The graph shows quantification of telomerase activity in MDSCs isolated from dKO and *mdx* mice. Error bars indicate 'mean ± SD'. $^*P < 0.05$. In (A), all scale bars = 50 μm.

however, they exhibit only a mild dystrophic phenotype (63). It is believed that *mdx* mice compensate for the lack of dystrophin through the upregulation of other proteins, such as utrophin (64). In this study, we demonstrated that the dystrophin/utrophin double knock-out mouse more closely recapitulates the DMD phenotype than the *mdx* model as evidenced by severe, progressive loss of muscle function, which is consistent with dKO models developed by other groups (50,51). Histopathologic analysis of dKO muscle sections revealed many of the characteristic features seen in DMD muscle biopsies, including variations in muscle fiber size, infiltration of inflammatory cells, the presence of necrotic fibers and calcium deposits and replacement of functional tissue with fibrotic tissue. Many of the other clinical features seen in the dKO mice, such as marked myopathy, joint contractures, kyphosis, loss of body weight, impaired muscle function and premature death (6–8 weeks), are all similar to what is observed in DMD patients. Of note, this is also similar to what is seen in *mdx/mTRG2* mice, a recently reported DMD model that exhibits rapid muscle stem cell exhaustion due to telomere shortening (52); however, these *mdx/mTRG2* mice have a much longer lifespan than the dKO mice (52). Given the important differences between the diaphragm and gastrocnemius muscles, we investigated and compared the histopathology of both muscles. Similar to what was reported in *mdx* mice, more muscle damage, greater cellular infiltration, increased fibrosis and reduced muscle regeneration (central nucleated myofibers) were found in the dKO diaphragm, compared with the dKO gastrocnemius, similar to what was reported in *mdx* mice (54,65–67). One notable exception to this trend at 6–8 weeks of age was a reduction in necrotic fibers in the diaphragm of the dKO mice, compared with the gastrocnemius muscle. This can be explained as a consequence of extensive myofiber loss and replacement with fibrosis and fat tissue in dKO diaphragm. As utrophin has been knocked out in this dKO animal model, the genotype is not the same as DMD, which only lacks dystrophin, yet, the dKO mice show most of the clinical features of DMD. Since many studies have shown that utrophin deficient mice are healthy and show no signs of weakness, living up to 2 years of age (68), it is unlikely that dKO abnormalities are caused primarily by utrophin deficiency.

We have proposed that the severe muscle wasting phenotype observed in this dKO mouse model is due to the impaired function of the MPC pools. Here we determined, both *in vitro* and *in vivo,* that the MPCs, including satellite cells, early myogenic progenitors (MDSCs) and myoblasts from aged dKO mice, are defective. *In vivo*, we confirmed that there was a rapid decline in satellite cell number during the progression of the disease in dKO muscles from 5 days to 8 weeks of age, in contrast to that observed in *mdx* skeletal muscle. *In vitro*, the proliferation and differentiation defects were marked by a reduction in the

number of satellite cells derived from the dKO single muscle fibers, and also a reduction in the formation of MyHCf-positive myotubes from their progeny in culture. MDSCs isolated from 6-week-old dKO mice also exhibited deficiencies in their proliferation and differentiation capacities, including the myogenic, adipogenic, osteogenic and chondrogenic lineages, and a reduction in their oxidative stress resistance. These data obtained from the dKO mouse model differ from the data obtained from the *mdx/mTRG2* mouse model. In contrast to our dKO mice, *mdx/mTRG2* mice show no alterations in satellite cell number per myofiber at 8 weeks of age (52), and do not demonstrate a markedly reduced number of satellite cells until the mice reach 60 weeks of age, indicating that MPC depletion appears at a much earlier age in the dKO mice than the *mdx/mTRG2* mouse model.

Further *in vivo* histologic analysis revealed that the amount of inflammatory infiltration substantially increased in the muscles of the dKO mice from 4 to 8 weeks of age, while the number of newly regenerated muscle fibers was significantly reduced during the same period, indicating an inability of the muscle to efficiently regenerate after injury. Similar to DMD patients, we observed a large amount of variability between the dKO mice; however, the occurrence of severe muscle histopathology was always associated with the depletion of the MPC pools. When taken together, this study demonstrated both *in vitro* and *in vivo* that MPCs isolated from dKO mice suffer from severe functional defects and that the progressive loss of MPCs plays a major role in determining the severity of the dystrophic phenotype. Indeed, the concept of stem cell exhaustion as a potential cause for the rapid progression of muscle weakness in DMD has been reported (35). Thus, we believe that the dKO model represents an excellent murine model of muscle stem cell exhaustion, allowing for the study of potential therapies for treating DMD patients.

There are several mechanisms that may contribute to MPC depletion and the severe phenotype of dKO mice. A study from the group of Andrew S. Brack demonstrated that increased FGF signaling is a major contributor to the loss of stem cell quiescence and is possibly implicated in stem cell depletion during aging under homeostatic conditions (59). Both real-time PCR and immunostaining showed that an upregulation of FGF2 expression is observed as early as 6–8 weeks of age in the dKO mice, whereas age-matched WT and *mdx* muscles did not express FGF2 until the mice reached 2 years of age. The reason for the increase in FGF2 expression is unknown, but this may contribute to the muscle stem cell depletion observed in dKO mice. Strategies to prevent chronic FGF2 production or repress FGF signaling may reduce stem cell loss during normal aging, but may not have beneficial effects on progressive muscle diseases, as FGF2 expression is also required for myoblast proliferation, differentiation and muscle regeneration following skeletal muscle injury (69,70).

Recent studies have also shown that muscle cells isolated from DMD patients have shorter telomeres than cells isolated from healthy individuals (60,71). Helen M. Blau's group showed that dystrophin deficiency, coupled with telomere dysfunction, recapitulated the severe dystrophic phenotype characteristic of muscular dystrophy in humans (52). This study provided evidence that telomere shortening, specifically in MPCs, leads to muscle stem cell exhaustion and the occurrence of the dystrophic histopathology. Moreover, it has also been reported that both muscle stem cell exhaustion and senescence could be the result of impaired telomerase activity (52,61,62). We tested our hypothesis that the muscle progenitor stem cell defect present in the dKO mice was also associated with a reduction in telomerase activity. Indeed, we found that the telomerase activity in dKO MDSCs was significantly reduced when compared with MDSCs isolated from age-matched WT and *mdx* mice. Reduced telomerase activity in dKO MDSCs could lead to defective cell proliferation, resistance to stress and muscle regeneration potentials. Taken together, we believe that both overexpression of FGF2 and a reduction in telomerase activity in dKO MDSCs plays a role in the rapid depletion of the dKO MPC pools, which ultimately results in the severe dystrophic phenotype observed in this model of DMD.

The data presented in the current study further validates that the dKO mouse model, when compared with the *mdx* mouse model, more closely recapitulates the severe phenotype observed in DMD patients. Moreover, the causative mechanism for the rapid occurrence of the dystrophic phenotype in the dKO mice and DMD patients may be related to a rapid depletion of the MPC pools. Therefore, alleviating MPC depletion could represent an approach to delay the onset of the histopathologies associated with DMD patients.

MATERIALS AND METHODS

Animals

dKO mice were generated by crossing (*utr*+/−; *dys*−/−) mice, which were obtained by crossing *utr*−/− and *mdx* mice (50) in our lab (42,72). WT mice (C57BL/10J) were ordered from Jackson Laboratories. All animal protocols used for these experiments were approved by the University of Pittsburgh's Animal Care and Use Committee.

Isolation of MDSCs from WT, *mdx* and dKO mice

The mice were sacrificed at 5 days and 6–8 weeks of age, and MDSC isolation was performed as previously described via a modified preplate technique (73,74). Briefly, the skeletal muscle tissue was minced and processed through a series of enzymatic dissociations: 0.2% of collagenase type XI (C7657, Sigma-Aldrich) for 1 h, 2.4 units/ml of dispase (17105-041, Invitrogen) for 45 min and 0.1% of trypsin–EDTA (15400-054, Invitrogen) for 30 min at 37°C. After enzymatic dissociation, the muscle cells were centrifuged and resuspended in proliferation medium (Dulbecco's modified Eagle's medium (DMEM, 11995-073, Invitrogen) supplemented with 10% fetal bovine serum (FBS, 10437–028, Invitrogen), 10% horse serum (HS, 26050-088, Invitrogen), 0.5% chicken embryo extract (CEE, CE650T-10, Accurate Chemical Co.) and 1% penicillin-streptomycin (15140-122, Invitrogen). The cells were then plated on collagen type I (C9791, Sigma-Aldrich) coated flasks. Different populations of muscle-derived cells were isolated based on their variable adhesion characteristics. After 7 days, late preplate populations (slow-adhering cells), which have previously been described to contain the MDSC fraction of cells, were obtained and cultured in proliferation medium (29).

Flow cytometry and cell sorting analyses

Fluorescence-activated cell sorting (FACS Aria II SORP; BD) was used to analyze the expression of CD34, Sca-1 (stem cell antigen-1) and CD45. Mice were sacrificed at 5 days and 6–8 weeks of age, and muscle cell isolation was performed as described above, using the modified preplate technique (73,74). After enzymatic dissociation, the muscle cells were centrifuged, resuspended in proliferation medium and then plated on collagen type I coated flasks. After 24 h, the floating cells, which contain the myogenic progenitor cells, were collected, centrifuged, washed with PBS containing 2% FBS and counted. The cell suspension was divided into equal aliquots and centrifuged, and then placed on ice and resuspended in a 1 : 10 dilution of mouse serum (M5905, Sigma-Aldrich) in PBS. The suspensions were incubated for 10 min. FITC-conjugated rat anti-CD34 (553733, BD), PE-conjugated rat anti-Sca-1(553108, BD) and APC-conjugated rat anti-CD45 (729744, Invitrogen) were added to each tube and incubated for an additional 30 min. Just before analysis, propidium iodide (PI, 556463, BD) was added to each tube for dead cell exclusion and live cell events were collected and analyzed. CD34+/Sca-1−/CD45− cells were sorted after analysis. A single color antibody was used to optimize fluorescence compensation settings for multicolor analyses and sorts.

Single-fiber isolation

dKO and *mdx* mice were sacrificed at 6–8 weeks of age, and the extensor digitorum longus (EDL) muscles were isolated and incubated in a solution of 0.2% collagenase type I (C5894, Sigma-Aldrich) for 50 min at 35°C while shaking at 40 rpm. When the muscles were sufficiently digested, they were triturated with heat polished glass pipettes to liberate single fibers. The muscle fibers were then transferred to a matrigel-coated (354234, Fisher) 24-well plate with proliferation medium (one fiber/well). The proliferative potential of MPCs derived from myofibers was analyzed after 4 days of culture by manually counting the number of desmin-positive cells that migrated from the isolated myofiber (number of MPCs per field of view per fiber).

In vitro assessment of cell proliferation

To compare the proliferative potential of the dKO MDSCs with that of WT and *mdx* MDSCs, we used a previously described Live Cell Imaging system (LCI) (Kairos Instruments LLC) (58,75). Bright field images were taken at 100× magnification at 10 min intervals over a 72-hour period in three fields of view per well, with three wells per population. Proliferation was assessed by manually counting the number of cells per field of view over 60 h.

Myogenic differentiation assay and fast myosin heavy chain staining

The cells were plated on 24-well plates (30 000 cells/well) in DMEM supplemented with 2% FBS to stimulate myotube formation. Three days after plating, immunocytochemical staining for fast myosin heavy chain (MyHCf) was performed. After rinsing two times with PBS, cells were fixed for 5 min in cold methanol (−20°C), blocked with 10% horse serum (S2000, Vector) for 1 h and then incubated with a mouse anti-MyHCf (M4276, 1 : 250; Sigma-Aldrich) antibody for 2 h at RT. The primary antibody was detected with an Alexa 594-conjugated antimouse IgG antibody (A21203, 1 : 500; molecular probes) for 30 min. The nuclei were revealed by 4,6-diamidino-2-phenylindole (DAPI, D9542, 100 ng/ml, Sigma-Aldrich) staining. The percentage of differentiated myotubes was quantified as the number of nuclei in MyHCf-positive myotubes relative to the total number of nuclei. This method was also used for analyzing myotube formation from single muscle fibers.

Survival analyses of MDSCs

Cells were exposed to oxidative stress by treatment with 400 μM hydrogen peroxide. In order to visualize cell death, the DNA-binding dye propidium iodide (PI) was added to the culture medium according to the manufacturer's protocol (BD Bioscience). Using the LCI system described above, 100× bright field and fluorescence images were taken at 10 min intervals over 24 h. Identifying the number of PI+ cells per field of view out of the total cell number determined the percentage of cell death over time.

Histochemistry and immunocytochemistry

In vitro: MPCs migrating off of single myofibers were stained for the myogenic marker desmin at 96 h after the fibers attached to the matrigel-coated (354234, Fisher) 24-well plates. The myofibers and cells were fixed in 5% formalin for 5 min and blocked with 10% donkey serum (017-000-121, Jackson ImmunoResearch) in PBS for 1 h at room temperature (RT). The fibers were incubated with rabbit antidesmin (D8281, 1 : 200; Sigma-Aldrich) for 3 h at RT, followed by PBS washes and incubation with a secondary antibody, donkey anti-rabbit IgG conjugated with Alexa Fluor 488 (A21206, 1 : 500, molecular probes), for 30 min. Nuclei were revealed with DAPI staining. Following desmin staining, the total number of desmin-positive cells that migrated from each of the myofibers was counted manually.

In vivo: muscle samples from 5-day-old, 4- to 8-week-old and 24-month-old mice were frozen in 2-methylbutane precooled in liquid nitrogen and stored at −80°C. H&E, alizarin red and trichrome staining were performed on 10 micrometer cryosections from the gastrocnemius and diaphragm, according to the manufacturer's instructions. Cryosections from the gastrocnemius and diaphragm were also fixed in a 1 : 1 cold (−20°C) acetone/methanol mixture for 5 min and preincubated in 10% donkey serum (017-000-121, Jackson ImmunoResearch) in PBS for 1 h at RT. Primary antibodies and their dilutions in PBS are listed below: rat anti-F4/80 (MCA497R, 1 : 500; Secrotec), rabbit anti-FGF (500-P152, 1 : 200; PeproTech) and rat anti-mouse IgG (BA-2000, 1 : 300; Vector). Fixed tissue sections were incubated with the primary antibodies for 3 h at RT, followed by PBS washes and incubation with secondary antibodies, Alexa594-conjugated donkey antirat IgG (A21209, 1 : 500; Molecular probes), Alexa594-conjugated donkey anti-rabbit IgG (A21207, 1 : 500; Molecular probes) and Alexa594-conjugated streptavidin (S-32356, 1 : 500; Molecular probes) for 30 min at RT. A MOM kit (Vector, Inc.) was used for Pax7 and embryonic myosin heavy chain (eMyHC) staining following the manufacturers protocol. The Pax7 and eMyHC primary abs and their

Table 1. Primers used for real-time PCR

Gene	Forward primers	Reverse primers	Location
Pax7	GTGCCCTCAGTGAGTTCGAT	CCACATCTGAGCCCTCATCC	499–667
FGF2	GGCTGCTGGCTTCTAAGTGT	GTCCCGTTTTGGATCCGAGT	463–615
eMyHC	GGAGGCTGATGAACAAGCCA	GCTAGAGGTGAAGTCACGGG	5696–5897
F4/80	CGGGGCTATGGGATGCATAA	TCAGCAACCTCGTGTCCTTG	2375–2564
β-Actin	TCAGAAGGACTCCTATGTGG	TCTTTGATGTCACGCACGAT	234–722

PBS dilutions are listed below: mouse anti-eMyHC (F1.652C, 1 : 50; Developmental Studies Hybridoma Bank) and mouse anti-Pax7 (1 : 100, Developmental Studies Hybridoma Bank). Cy3-streptavidin (GEPA43001, 1 : 500, Sigma-Aldrich) was added to act as the tertiary antibody, and the nuclei were stained with DAPI. All the stained sections were visualized on a Nikon Eclipse E800 fluorescence microscope. Ten random pictures per slide were taken and the number of Pax7+ cells and eMyHC+ myofibers were counted manually. F4/80+ macrophage infiltration areas, mouse IgG+ necrotic fibers and collage +fibrotic areas were measured and quantified [positive area per total muscle area (%)] using Northern Eclipse software.

Adipogenesis assay

A total of 60 000 MDSCs were cultured on 24-well collagen type I-coated plates for 21 days in adipogenic differentiation medium (PT-3004, Lonza). At 100% confluence, three cycles of induction/maintenance medium stimulated optimal adipogenic differentiation. Each cycle consisted of feeding the MDSCs with supplemented adipogenesis induction medium and cultured for 3 days followed by 1–3 days of culture in supplemented adipogenic maintenance medium. Then, MDSCs were tested for adipogenesis with AdipoRed reagent (NC9049267, 30 μl/ml, Fisher) following the manufacturer's protocols.

Osteogenesis assay

A total of 50 000 cells were cultured in osteogenic medium, control medium supplemented with dexamethasone (D2915, 0.1 μM, Sigma-Aldrich), ascorbic-acid-2-phosphate (A8960, 50 μg/ml, Sigma-Aldrich) and 10 mM B-glycerophosphate (BMP2, G6251, 100 ng/ml, Sigma-Aldrich). Cells were stained for calcium deposition (Alizarin Red) after 7 and 10 days of culture, respectively.

Chondrogenesis assay

MDSCs were centrifuged into pellets (250 000 cells/pellet) and cultured for 4 weeks in chondrogenic induction media (PT3003, 200 μl/pellet, Lonza) supplemented with 100 ng/ml BMP2 and 20 ng/ml TGFβ3 (PHG9305, 20 ng/ml, Invitrogen). Pellets were frozen in embedding medium and cryosectioned. The sections were then stained with alcian blue to confirm chondrogenesis. To further confirm the pellet chondrogenecity, a GAG assay was performed to verify the presence of proteoglycans.

Real-time PCR

Total RNA from muscle tissue of 4- to 8-week-old mice was isolated using TRizol reagent (Invitrogen) and reverse transcribed using a Maxima first strand cDNA synthesis kit (Fermentas) according to the manufacturer's protocol. Real-time PCR was carried out using the Maxima SYBR® Green Assay kit (Fermentas) using an iQ5 thermocycler (Biorad). Primers were designed using PRIMER-Blast (NCBI) and can be found in Table 1. All the quantitative PCR results were normalized relative to β-actin.

Detection of telomerase activity in MDSCs

Telomerase activity in MDSCs was detected with a TeloTAGGG Telomerase PCR ELISA kit (11854666910, Roche) according the manufacturer's instructions. Briefly, MDSCs from 4-week-old *mdx* and dKO mice were processed with the lysis reagent provided in the kit to prepare cell extracts. Cell extracts were then used to conduct the telomeric repeat amplification protocol (TRAP reaction), generating PCR products with telomerase-specific six nucleotide increments (TTAGGG). The resulting quantity of PCR products depends on the telomerase activity in the cell extracts. The PCR products were then denatured and hybridized to a digoxigenin-(DIG)-labeled, telomeric repeat-specific detection probe. The PCR products were then detected using an antibody against digoxigenin (anti-DIG-POD). The signal intensity of the antibody was then read with an ELISA plate reader (Infinite M200, TECAN, Inc.).

Skeletal muscle functional measurements

Six- to eight-week-old animals were anesthetized with 2–3% isoflurane and maintained in a surgical plane during the procedure with 1.5% isoflurane. The lower hind limbs were shaved and the animals were placed on an *in situ* muscle physiology test apparatus (Model 806-B, Aurora Scientific) with only the right hind limb being tested. The animal was laid in a supine position and the foot was secured to the force plate with adhesive tape. The knee was positioned and secured at 90° of flexion and the ankle was at 0° of flexion. Twenty-seven gauge needle electrodes were placed intramuscularly into the tibialis anterior. Force–frequency curves were generated by stimulating the muscles with 9 V at varying frequencies from 1 Hz up to 200 Hz with a 2 min rest between each of the frequency stimulations. Data were recorded and analyzed with the DMC software (Aurora Scientific).

Statistical analysis

All results are given as the mean ± standard deviation (SD). Means from dKO, *mdx* and WT mice were compared using Student's *t*-test. Differences were considered statistically significant when the *P*-value was < 0.05.

SUPPLEMENTARY MATERIAL

Supplementary Material is available at *HMG* online.

ACKNOWLEDGEMENTS

We thank James Cummins and Bria King for their editorial assistance.

Conflict of Interest statement. The authors do not have conflicts of interest to disclose other than the corresponding author who receives consulting fees and royalties from Cook MyoSite Inc.

FUNDING

This work was supported in part by grants from the National Institutes of Health (NIH 1P01AG043376-01A1) and the Department of Defense (W81-XWH-09-1-0658) awarded to J.H. as well as the Henry J. Mankin Endowed Chair at the University of Pittsburgh.

REFERENCES

1. Durbeej, M. and Campbell, K.P. (2002) Muscular dystrophies involving the dystrophin-glycoprotein complex: an overview of current mouse models. *Curr. Opin. Genet. Dev.*, **12**, 349–361.
2. Tinsley, J.M., Blake, D.J., Zuellig, R.A. and Davies, K.E. (1994) Increasing complexity of the dystrophin-associated protein complex. *Proc. Natl. Acad. Sci. USA*, **91**, 8307–8313.
3. Blake, D.J., Weir, A., Newey, S.E. and Davies, K.E. (2002) Function and genetics of dystrophin and dystrophin-related proteins in muscle. *Physiol. Rev.*, **82**, 291–329.
4. Petrof, B.J., Shrager, J.B., Stedman, H.H., Kelly, A.M. and Sweeney, H.L. (1993) Dystrophin protects the sarcolemma from stresses developed during muscle contraction. *Proc. Natl. Acad. Sci. USA*, **90**, 3710–3714.
5. Weller, B., Karpati, G. and Carpenter, S. (1990) Dystrophin-deficient mdx muscle fibers are preferentially vulnerable to necrosis induced by experimental lengthening contractions. *J. Neurol. Sci.*, **100**, 9–13.
6. Dellorusso, C., Crawford, R.W., Chamberlain, J.S. and Brooks, S.V. (2001) Tibialis anterior muscles in mdx mice are highly susceptible to contraction-induced injury. *J. Muscle Res. Cell Motil.*, **22**, 467–475.
7. Arahata, K. (1991) Dystrophin abnormality in progressive muscular dystrophy--a review article. *Acta Paediatr. Jpn.*, **33**, 216–221.
8. Lapidos, K.A., Kakkar, R. and McNally, E.M. (2004) The dystrophin glycoprotein complex: signaling strength and integrity for the sarcolemma. *Circ. Res.*, **94**, 1023–1031.
9. Hoffman, E.P., Brown, R.H. Jr and Kunkel, L.M. (1987) Dystrophin: the protein product of the Duchenne muscular dystrophy locus. *Cell*, **51**, 919–928.
10. Mauro, A. (1961) Satellite cell of skeletal muscle fibers. *J Biophys Biochem Cytol*, **9**, 493–495.
11. Montarras, D., Morgan, J., Collins, C., Relaix, F., Zaffran, S., Cumano, A., Partridge, T. and Buckingham, M. (2005) Direct isolation of satellite cells for skeletal muscle regeneration. *Science*, **309**, 2064–2067.
12. Zammit, P.S., Relaix, F., Nagata, Y., Ruiz, A.P., Collins, C.A., Partridge, T.A. and Beauchamp, J.R. (2006) Pax7 and myogenic progression in skeletal muscle satellite cells. *J. Cell Sci.*, **119**, 1824–1832.
13. Fukada, S., Ma, Y., Ohtani, T., Watanabe, Y., Murakami, S. and Yamaguchi, M. (2013) Isolation, characterization, and molecular regulation of muscle stem cells. *Front. Physiol.*, **4**, 317.
14. Pannerec, A., Formicola, L., Besson, V., Marazzi, G. and Sassoon, D.A. (2013) Defining skeletal muscle resident progenitors and their cell fate potentials. *Development*, **140**, 2879–2891.
15. Zheng, B., Cao, B., Crisan, M., Sun, B., Li, G., Logar, A., Yap, S., Pollett, J.B., Drowley, L., Cassino, T. *et al.* (2007) Prospective identification of myogenic endothelial cells in human skeletal muscle. *Nat. Biotechnol.*, **25**, 1025–1034.
16. Benchaouir, R., Rameau, P., Decraene, C., Dreyfus, P., Israeli, D., Pietu, G., Danos, O. and Garcia, L. (2004) Evidence for a resident subset of cells with SP phenotype in the C2C12 myogenic line: a tool to explore muscle stem cell biology. *Exp. Cell Res.*, **294**, 254–268.
17. Mitchell, K.J., Pannerec, A., Cadot, B., Parlakian, A., Besson, V., Gomes, E.R., Marazzi, G. and Sassoon, D.A. (2010) Identification and characterization of a non-satellite cell muscle resident progenitor during postnatal development. *Nat. Cell Biol.*, **12**, 257–266.
18. Galvez, B.G., Sampaolesi, M., Brunelli, S., Covarello, D., Gavina, M., Rossi, B., Constantin, G., Torrente, Y. and Cossu, G. (2006) Complete repair of dystrophic skeletal muscle by mesoangioblasts with enhanced migration ability. *J. Cell Biol.*, **174**, 231–243.
19. Dellavalle, A., Sampaolesi, M., Tonlorenzi, R., Tagliafico, E., Sacchetti, B., Perani, L., Innocenzi, A., Galvez, B.G., Messina, G., Morosetti, R. *et al.* (2007) Pericytes of human skeletal muscle are myogenic precursors distinct from satellite cells. *Nat. Cell Biol.*, **9**, 255–267.
20. Dellavalle, A., Maroli, G., Covarello, D., Azzoni, E., Innocenzi, A., Perani, L., Antonini, S., Sambasivan, R., Brunelli, S., Tajbakhsh, S. *et al.* (2011) Pericytes resident in postnatal skeletal muscle differentiate into muscle fibres and generate satellite cells. *Nat Commun*, **2**, 499.
21. Pannerec, A., Marazzi, G. and Sassoon, D. (2012) Stem cells in the hood: the skeletal muscle niche. *Trends Mol. Med.*, **18**, 599–606.
22. Brzoska, E., Kowalewska, M., Markowska-Zagrajek, A., Kowalski, K., Archacka, K., Zimowska, M., Grabowska, I., Czerwinska, A.M., Czarnecka-Gora, M., Streminska, W. *et al.* (2012) Sdf-1 (CXCL12) improves skeletal muscle regeneration via the mobilisation of Cxcr4 and CD34 expressing cells. *Biol. Cell.*, **104**, 722–737.
23. Asakura, A., Seale, P., Girgis-Gabardo, A. and Rudnicki, M.A. (2002) Myogenic specification of side population cells in skeletal muscle. *J. Cell Biol.*, **159**, 123–134.
24. De Angelis, L., Berghella, L., Coletta, M., Lattanzi, L., Zanchi, M., Cusella-De Angelis, M.G., Ponzetto, C. and Cossu, G. (1999) Skeletal myogenic progenitors originating from embryonic dorsal aorta coexpress endothelial and myogenic markers and contribute to postnatal muscle growth and regeneration. *J. Cell Biol.*, **147**, 869–878.
25. Tamaki, T., Okada, Y., Uchiyama, Y., Tono, K., Masuda, M., Nitta, M., Hoshi, A. and Akatsuka, A. (2008) Skeletal muscle-derived CD34+/45− and CD34−/45− stem cells are situated hierarchically upstream of Pax7+ cells. *Stem Cells Dev*, **17**, 653–667.
26. Lee, J.Y., Qu-Petersen, Z., Cao, B., Kimura, S., Jankowski, R., Cummins, J., Usas, A., Gates, C., Robbins, P., Wernig, A. *et al.* (2000) Clonal isolation of muscle-derived cells capable of enhancing muscle regeneration and bone healing. *J. Cell Biol.*, **150**, 1085–1100.
27. Torrente, Y., Tremblay, J.P., Pisati, F., Belicchi, M., Rossi, B., Sironi, M., Fortunato, F., El Fahime, M., D'Angelo, M.G., Caron, N.J. *et al.* (2001) Intraarterial injection of muscle-derived CD34(+)Sca-1(+) stem cells restores dystrophin in mdx mice. *J. Cell Biol.*, **152**, 335–348.
28. Vella, J.B., Thompson, S.D., Bucsek, M.J., Song, M. and Huard, J. (2011) Murine and human myogenic cells identified by elevated aldehyde dehydrogenase activity: implications for muscle regeneration and repair. *PLoS One*, **6**, e29226.
29. Qu-Petersen, Z., Deasy, B., Jankowski, R., Ikezawa, M., Cummins, J., Pruchnic, R., Mytinger, J., Cao, B., Gates, C., Wernig, A. *et al.* (2002) Identification of a novel population of muscle stem cells in mice: potential for muscle regeneration. *J. Cell Biol.*, **157**, 851–864.
30. Usas, A. and Huard, J. (2007) Muscle-derived stem cells for tissue engineering and regenerative therapy. *Biomaterials*, **28**, 5401–5406.
31. Kuroda, R., Usas, A., Kubo, S., Corsi, K., Peng, H., Rose, T., Cummins, J., Fu, F.H. and Huard, J. (2006) Cartilage repair using bone morphogenetic protein 4 and muscle-derived stem cells. *Arthritis Rheum.*, **54**, 433–442.
32. Cao, B., Zheng, B., Jankowski, R.J., Kimura, S., Ikezawa, M., Deasy, B., Cummins, J., Epperly, M., Qu-Petersen, Z. and Huard, J. (2003) Muscle stem cells differentiate into haematopoietic lineages but retain myogenic potential. *Nat. Cell Biol.*, **5**, 640–646.
33. McLoon, L.K. (2008) Focusing on fibrosis: halofuginone-induced functional improvement in the mdx mouse model of Duchenne muscular dystrophy. *Am. J. Physiol. Heart Circ. Physiol.*, **294**, H1505–H1507.
34. Morgan, J.E. and Zammit, P.S. (2010) Direct effects of the pathogenic mutation on satellite cell function in muscular dystrophy. *Exp. Cell Res.*, **316**, 3100–3108.
35. Blau, H.M., Webster, C. and Pavlath, G.K. (1983) Defective myoblasts identified in Duchenne muscular dystrophy. *Proc. Natl. Acad. Sci. USA*, **80**, 4856–4860.

36. Webster, C. and Blau, H.M. (1990) Accelerated age-related decline in replicative life-span of Duchenne muscular dystrophy myoblasts: implications for cell and gene therapy. *Somat. Cell Mol. Genet.*, **16**, 557–565.
37. Bulfield, G., Siller, W.G., Wight, P.A. and Moore, K.J. (1984) x chromosome-linked muscular dystrophy (mdx) in the mouse. *Proc. Natl. Acad. Sci. USA*, **81**, 1189–1192.
38. Ryder-Cook, A.S., Sicinski, P., Thomas, K., Davies, K.E., Worton, R.G., Barnard, E.A., Darlison, M.G. and Barnard, P.J. (1988) Localization of the mdx mutation within the mouse dystrophin gene. *EMBO J.*, **7**, 3017–3021.
39. DiMario, J.X., Uzman, A. and Strohman, R.C. (1991) Fiber regeneration is not persistent in dystrophic (MDX) mouse skeletal muscle. *Dev. Biol.*, **148**, 314–321.
40. Straub, V., Rafael, J.A., Chamberlain, J.S. and Campbell, K.P. (1997) Animal models for muscular dystrophy show different patterns of sarcolemmal disruption. *J. Cell Biol.*, **139**, 375–385.
41. Khouzami, L., Bourin, M.C., Christov, C., Damy, T., Escoubet, B., Caramelle, P., Perier, M., Wahbi, K., Meune, C., Pavoine, C. *et al.* (2010) Delayed cardiomyopathy in dystrophin deficient mdx mice relies on intrinsic glutathione resource. *Am. J. Pathol.*, **177**, 1356–1364.
42. Isaac, C., Wright, A., Usas, A., Li, H., Tang, Y., Mu, X., Greco, N., Dong, Q., Vo, N., Kang, J. *et al.* (2013) Dystrophin and utrophin 'double knockout' dystrophic mice exhibit a spectrum of degenerative musculoskeletal abnormalities. *J. Orthop. Res.*, **31**, 343–349.
43. Kornegay, J.N., Childers, M.K., Bogan, D.J., Bogan, J.R., Nghiem, P., Wang, J., Fan, Z., Howard, J.F. Jr, Schatzberg, S.J., Dow, J.L. *et al.* (2012) The paradox of muscle hypertrophy in muscular dystrophy. *Phys. Med. Rehabil. Clin. N. Am.*, **23**, 149–172, xii.
44. Nguyen, T.M., Le, T.T., Blake, D.J., Davies, K.E. and Morris, G.E. (1992) Utrophin, the autosomal homologue of dystrophin, is widely-expressed and membrane-associated in cultured cell lines. *FEBS Lett*, **313**, 19–22.
45. Ferretti, R., Neto, H.S. and Marques, M.J. (2011) Expression of utrophin at dystrophin-deficient neuromuscular synapses of mdx mice: a study of protected and affected muscles. *Anat Rec (Hoboken)*, **294**, 283–286.
46. Baban, D. and Davies, K.E. (2008) Microarray analysis of mdx mice expressing high levels of utrophin: therapeutic implications for dystrophin deficiency. *Neuromuscul. Disord.*, **18**, 239–247.
47. Bewick, G.S., Nicholson, L.V., Young, C., O'Donnell, E. and Slater, C.R. (1992) Different distributions of dystrophin and related proteins at nerve-muscle junctions. *Neuroreport*, **3**, 857–860.
48. Law, D.J., Allen, D.L. and Tidball, J.G. (1994) Talin, vinculin and DRP (utrophin) concentrations are increased at mdx myotendinous junctions following onset of necrosis. J. Cell Sci., **107**(Pt 6), 1477–1483.
49. Deol, J.R., Danialou, G., Larochelle, N., Bourget, M., Moon, J.S., Liu, A.B., Gilbert, R., Petrof, B.J., Nalbantoglu, J. and Karpati, G. (2007) Successful compensation for dystrophin deficiency by a helper-dependent adenovirus expressing full-length utrophin. *Mol. Ther.*, **15**, 1767–1774.
50. Deconinck, A.E., Rafael, J.A., Skinner, J.A., Brown, S.C., Potter, A.C., Metzinger, L., Watt, D.J., Dickson, J.G., Tinsley, J.M. and Davies, K.E. (1997) Utrophin-dystrophin-deficient mice as a model for Duchenne muscular dystrophy. *Cell*, **90**, 717–727.
51. Grady, R.M., Teng, H., Nichol, M.C., Cunningham, J.C., Wilkinson, R.S. and Sanes, J.R. (1997) Skeletal and cardiac myopathies in mice lacking utrophin and dystrophin: a model for Duchenne muscular dystrophy. *Cell*, **90**, 729–738.
52. Sacco, A., Mourkioti, F., Tran, R., Choi, J., Llewellyn, M., Kraft, P., Shkreli, M., Delp, S., Pomerantz, J.H., Artandi, S.E. *et al.* (2010) Short telomeres and stem cell exhaustion model Duchenne muscular dystrophy in mdx/mTR mice. *Cell*, **143**, 1059–1071.
53. Lu, A., Cummins, J.H., Pollett, J.B., Cao, B., Sun, B., Rudnicki, M.A. and Huard, J. (2008) Isolation of myogenic progenitor populations from Pax7-deficient skeletal muscle based on adhesion characteristics. *Gene Ther.*, **15**, 1116–1125.
54. Stupka, N., Michell, B.J., Kemp, B.E. and Lynch, G.S. (2006) Differential calcineurin signalling activity and regeneration efficacy in diaphragm and limb muscles of dystrophic mdx mice. *Neuromuscul. Disord.*, **16**, 337–346.
55. Kallestad, K.M., Hebert, S.L., McDonald, A.A., Daniel, M.L., Cu, S.R. and McLoon, L.K. (2011) Sparing of extraocular muscle in aging and muscular dystrophies: a myogenic precursor cell hypothesis. *Exp. Cell Res.*, **317**, 873–885.
56. Jankowski, R.J., Haluszczak, C., Trucco, M. and Huard, J. (2001) Flow cytometric characterization of myogenic cell populations obtained via the preplate technique: potential for rapid isolation of muscle-derived stem cells. *Hum. Gene Ther.*, **12**, 619–628.
57. Deasy, B.M., Gharaibeh, B.M., Pollett, J.B., Jones, M.M., Lucas, M.A., Kanda, Y. and Huard, J. (2005) Long-term self-renewal of postnatal muscle-derived stem cells. *Mol. Biol. Cell*, **16**, 3323–3333.
58. Chirieleison, S.M., Bissell, T.A., Scelfo, C.C., Anderson, J.E., Li, Y., Koebler, D.J. and Deasy, B.M. (2011) Automated live cell imaging systems reveal dynamic cell behavior. *Biotechnol. Prog.*, **27**, 913–924.
59. Chakkalakal, J.V., Jones, K.M., Basson, M.A. and Brack, A.S. (2012) The aged niche disrupts muscle stem cell quiescence. *Nature*, **490**, 355–360.
60. Mouly, V., Aamiri, A., Bigot, A., Cooper, R.N., Di Donna, S., Furling, D., Gidaro, T., Jacquemin, V., Mamchaoui, K., Negroni, E. *et al.* (2005) The mitotic clock in skeletal muscle regeneration, disease and cell mediated gene therapy. *Acta Physiol. Scand.*, **184**, 3–15.
61. Zhu, C.H., Mouly, V., Cooper, R.N., Mamchaoui, K., Bigot, A., Shay, J.W., Di Santo, J.P., Butler-Browne, G.S. and Wright, W.E. (2007) Cellular senescence in human myoblasts is overcome by human telomerase reverse transcriptase and cyclin-dependent kinase 4: consequences in aging muscle and therapeutic strategies for muscular dystrophies. *Aging Cell*, **6**, 515–523.
62. Wootton, M., Steeghs, K., Watt, D., Munro, J., Gordon, K., Ireland, H., Morrison, V., Behan, W. and Parkinson, E.K. (2003) Telomerase alone extends the replicative life span of human skeletal muscle cells without compromising genomic stability. *Hum. Gene Ther.*, **14**, 1473–1487.
63. Lefaucheur, J.P., Pastoret, C. and Sebille, A. (1995) Phenotype of dystrophinopathy in old mdx mice. *Anat. Rec.*, **242**, 70–76.
64. Matsumura, K., Ervasti, J.M., Ohlendieck, K., Kahl, S.D. and Campbell, K.P. (1992) Association of dystrophin-related protein with dystrophin-associated proteins in mdx mouse muscle. *Nature*, **360**, 588–591.
65. Stedman, H.H., Sweeney, H.L., Shrager, J.B., Maguire, H.C., Panettieri, R.A., Petrof, B., Narusawa, M., Leferovich, J.M., Sladky, J.T. and Kelly, A.M. (1991) The mdx mouse diaphragm reproduces the degenerative changes of Duchenne muscular dystrophy. *Nature*, **352**, 536–539.
66. Tkatchenko, A.V., Le Cam, G., Leger, J.J. and Dechesne, C.A. (2000) Large-scale analysis of differential gene expression in the hindlimb muscles and diaphragm of mdx mouse. *Biochim. Biophys. Acta*, **1500**, 17–30.
67. Lang, J.M., Esser, K.A. and Dupont-Versteegden, E.E. (2004) Altered activity of signaling pathways in diaphragm and tibialis anterior muscle of dystrophic mice. *Exp. Biol. Med. (Maywood)*, **229**, 503–511.
68. Deconinck, A.E., Potter, A.C., Tinsley, J.M., Wood, S.J., Vater, R., Young, C., Metzinger, L., Vincent, A., Slater, C.R. and Davies, K.E. (1997) Postsynaptic abnormalities at the neuromuscular junctions of utrophin-deficient mice. *J. Cell Biol.*, **136**, 883–894.
69. Stratos, I., Madry, H., Rotter, R., Weimer, A., Graff, J., Cucchiarini, M., Mittlmeier, T. and Vollmar, B. (2011) Fibroblast growth factor-2-overexpressing myoblasts encapsulated in alginate spheres increase proliferation, reduce apoptosis, induce adipogenesis, and enhance regeneration following skeletal muscle injury in rats. *Tissue Eng Part A*, **17**, 2867–2877.
70. Neuhaus, P., Oustanina, S., Loch, T., Kruger, M., Bober, E., Dono, R., Zeller, R. and Braun, T. (2003) Reduced mobility of fibroblast growth factor (FGF)-deficient myoblasts might contribute to dystrophic changes in the musculature of FGF2/FGF6/mdx triple-mutant mice. *Mol. Cell. Biol.*, **23**, 6037–6048.
71. Decary, S., Hamida, C.B., Mouly, V., Barbet, J.P., Hentati, F. and Butler-Browne, G.S. (2000) Shorter telomeres in dystrophic muscle consistent with extensive regeneration in young children. *Neuromuscul. Disord.*, **10**, 113–120.
72. Wang, B., Li, J., Fu, F.H. and Xiao, X. (2009) Systemic human minidystrophin gene transfer improves functions and life span of dystrophin and dystrophin/utrophin-deficient mice. *J. Orthop. Res.*, **27**, 421–426.
73. Lavasani, M., Lu, A., Thompson, S.D., Robbins, P.D., Huard, J. and Niedernhofer, L.J. (2013) Isolation of muscle-derived stem/progenitor cells based on adhesion characteristics to collagen-coated surfaces. *Methods Mol. Biol.*, **976**, 53–65.
74. Gharaibeh, B., Lu, A., Tebbets, J., Zheng, B., Feduska, J., Crisan, M., Peault, B., Cummins, J. and Huard, J. (2008) Isolation of a slowly adhering cell fraction containing stem cells from murine skeletal muscle by the preplate technique. *Nat. Protoc.*, **3**, 1501–1509.
75. Deasy, B.M., Jankowski, R.J., Payne, T.R., Cao, B., Goff, J.P., Greenberger, J.S. and Huard, J. (2003) Modeling stem cell population growth: incorporating terms for proliferative heterogeneity. *Stem Cells*, **21**, 536–545.